Appl Magn Reson (2014) 45:1117–1126
DOI 10.1007/s00723-014-0603-x

Applied
Magnetic Resonance

Low-Temperature Molecular Motions in Phospholipid Bilayers in Presence of Glycerol as Studied by Spin-Echo EPR of Spin Labels

K. B. Konov · N. P. Isaev · S. A. Dzuba

Received: 30 June 2014 / Revised: 18 September 2014 / Published online: 1 October 2014

Abstract Glycerol is used as a cryoprotective agent to protect biological systems under freezing conditions. Electron spin echo (ESE) spectroscopy, a pulsed version of EPR, is capable of studying low-temperature molecular motions of nitroxide spin labels. ESE technique was applied to study molecular motions in phospholipid bilayers prepared from 1,2-dipalmitoyl-*sn*-glycero-3-phosphocholine (DPPC) with added spin-labeled lipids 1-palmitoyl-2-stearoyl-(*n*-DOXYL)-*sn*-glycero-3-phosphocholine (*n*-PCSL, *n* was optionally 5 or 16). Bilayers were hydrated (solvated) either in pure water or in a 1:1 v/v water–glycerol mixture. In the used ESE approach, there were studied stochastic (or diffusive) orientational vibrations of the molecule as a whole (i.e., stochastic molecular librations). The anisotropic contribution to the echo decay rate, W_{anis}, was measured, which is proportional, according to theory, to the product of the mean-squared angular amplitude $\langle\alpha^2\rangle$ and the correlation time τ_c. W_{anis} was found to be small below and to sharply increase above 200 K, for the both types of solvents and the both label positions. As compared with hydration by pure water, in presence of glycerol W_{anis} was larger for the 5th label position while for the 16th one it did not change. Also, for the 5th label position W_{anis} values were found to be nearly the same as those for a polar spin probe 3,4-dicarboxy-PROXYL which was separately added to the bilayer as a reference and which is assumed to be partitioned only into the solvating shell. These results indicate that motions at the surface of bilayer are governed by the motion of

K. B. Konov
Zavoisky Physical-Technical Institute, Russian Academy of Sciences, Kazan 420029, Russia

N. P. Isaev · S. A. Dzuba
Voevodsky Institute of Chemical Kinetics and Combustion,
Russian Academy of Sciences, Novosibirsk 630090, Russia

S. A. Dzuba (✉)
Novosibirsk State University, Novosibirsk 630090, Russia
e-mail: dzuba@kinetics.nsc.ru

solvating shell while motions in the bilayer interior occur independently. The relation of the obtained data with the dynamical transition phenomenon that is known for biological substances near 200 K from neutron scattering and Mössbauer absorption is discussed.

1 Introduction

Glycerol is known to protect biological membranes under extreme conditions, such as freezing and desiccation [1–5]. A variety of organisms accumulate glycerol to tolerate extreme environmental conditions [6–8]. Glycerol can stabilize the native structures of biomacromolecules [9, 10], regulate microviscosity [6, 7], prevent intracellular ice formation [4, 10–13]. A water–glycerol mixture is widely used as a cryoprotective liquid for conservation of human cells [14], as well as in different laboratory researches when cryogenic temperatures are required for implementation of the technique. However, the molecular mechanisms of the cryoprotective action of glycerol are not clear. To elucidate these mechanisms, structural and dynamical properties of biological systems in presence of glycerol should be studied at cryogenic temperatures.

Molecular motions in biological systems at low temperatures were widely investigated using Mössbauer spectroscopy (in iron-containing proteins) [15–17] and neutron scattering [18–30]. These techniques allow measuring the mean-squared displacement (MSD), $\langle r^2 \rangle$, of atoms experiencing vibrational motion. The obtained results show that biological systems undergo a dramatic change in their dynamic and/or structural properties at 180–230 K. At lower temperatures MSD has linear temperature dependence, which is consistent with harmonic vibrational motion. At higher temperatures the MSD temperature dependence becomes much steeper; the motion is considered here as anharmonic or diffusive. This transition is called dynamical transition, temperature where it occurs is denoted as T_d. Mössbauer spectroscopy probes the motion in the time scale of 10^{-7} s, neutron scattering is sensitive to a shorter pico- to nanosecond timescale. Dynamical transition was observed for different biological systems: proteins [15–23], DNAs [24], RNAs [25], small amino acids [26], biological membranes [27–30].

Except for neutron scattering and Mössbauer absorption, other techniques also are sensitive to the dynamical transition in biological media near 200 K. This transition can be detected by molecular dynamics (MD) simulations [31, 32], by Raman spectroscopy [33–35], by electron spin echo (ESE) of spin labels [35–40].

The dynamical transition in biomolecules is known to be strongly influenced by their solvating shells. In the glassy glycerol or water/glycerol surroundings, it was studied for proteins [20, 31, 32, 41, 42] and DNAs [24], using either neutron scattering [20, 24, 41, 42] or MD simulations [31, 32]. The dynamics of biomolecules was found to be coupled with that of the surrounding matrix, so the crucial role of the solvent mobility to activate thermal fluctuations was proposed.

Spin-label ESE is capable of detecting dynamical transition in biological systems [35–40] because the rate of spin relaxation observed with ESE is proportional to the mean-squared amplitude, $\langle \alpha^2 \rangle$, of nanosecond stochastic molecular orientational

vibrations (stochastic or diffusive molecular librations) [43, 44]. These stochastic molecular librations were suggested to have the same nature as anharmonic (or diffusive) vibrations detected above T_d in biological substances by neutron scattering and Mössbauer spectroscopy [45]. In this work, we employed ESE technique to study molecular motions in spin-labeled phospholipid bilayers hydrated (solvated) in the presence of glycerol.

2 Experimental

Phosphatidylcholines 1,2-dipalmitoyl-*sn*-glycero-3-phosphocholine (DPPC) and spin-labeled 1-palmitoyl-2-stearoyl-(*n*-DOXYL)-*sn*-glycero-3-phosphocholine (*n*-PCSL, $n = 5$ or 16) were obtained from Avanti Polar Lipids (Birmingham, AL). The chemical structures of the lipids are given below:

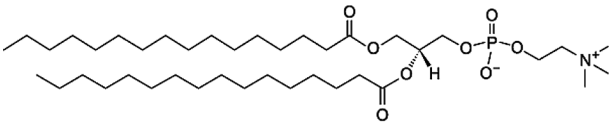

DPPC

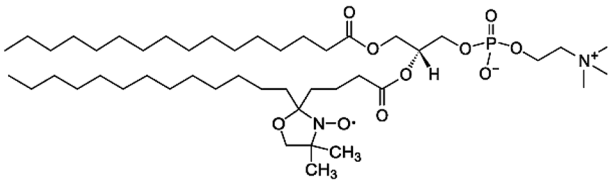

5-PCSL

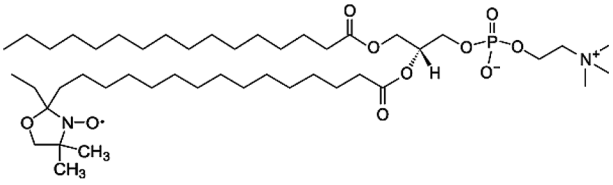

16-PCSL

Lipids *n*-PCSL and DPPC were co-dissolved in the molar ratio of 1:100 in chloroform. The solvent was removed by nitrogen flow followed by 12 h storage under vacuum (10^{-2} bar). The obtained *n*-PCSL/DPPC samples were hydrated for 4 h at temperatures above the gel-to-fluid phase transition temperature by adding

either pure water or a 1:1 v/v water/glycerol mixture. Glycerol (Reakhim, Moscow) was distilled, water was bidistilled. The proportion between the total amount of lipids and the solvent added was 1:4 w/w. The samples were put into quartz tubes of 4.8 mm o.d., stored at 5 °C for 12 h and then frozen by immersion in liquid nitrogen just before measurements.

In some experiments instead of spin-labeled lipids a small spin probe nitroxide trans-I-oxyl-2,2,5,5-tetramethyl-3,4-dicarboxypyrrolidine (3,4-dicarboxy-proxyl) (gift from Dr. I. A. Kirilyuk) was used, added in a concentration of 1 mM.

An ELEXSYS E580 9-GHz FT-EPR spectrometer (Bruker, Germany) equipped with a dielectric resonator (Bruker ER 4118X-MD5) inside an Oxford Instruments CF 935 cryostat was used. To acquire continuous-wave electron paramagnetic resonance (CW EPR) spectra, the resonator was adjusted to a high quality. The incident microwave power was controlled to ensure absence of saturation of EPR spectra. In pulse experiments, the resonator was overcoupled to provide a short ring time ($\sim$100 ns). A two-pulse ESE sequence, *16 ns pulse-τ–32 ns pulse-τ-echo*, was used. The pulse amplitudes were adjusted to provide $\pi/2$ and π turning angles for the first and second pulses, respectively. To acquire ESE decay time traces, the time delay τ was scanned with a step of 4 ns. All data treatment was performed on a PC.

The cryostat was cooled by flowing cold nitrogen gas. The sample temperature was controlled with an accuracy of $\pm$0.5 K.

3 Results

The EPR spectrum of nitroxide consists of three hyperfine components corresponding to three projections m of the nitrogen nuclear spin ($I = 1$) on its quantization axis, $m = 0, \pm 1$, see inset to Fig. 1. The central component ($m = 0$) in the spectrum is the narrowest one because it is not influenced by anisotropy of hyperfine interactions. The high-field component ($m = -1$) is the most anisotropic and thus it is the broadest. Echo decays were obtained at the two field positions—in the maximum of central component and in the middle of the high-field one, as it is shown in Fig. 1. The obtained time traces (typical original examples are given in the inset to Fig. 1) were divided by each other, to eliminate all field-independent contributions to transverse spin relaxation. Note that oscillations seen on the original time traces arise because of hyperfine interactions of electron spin with nearby protons—that is the so-called ESE envelope modulation (ESEEM) phenomenon. The division results in extraction of a pure contribution to spin relaxation from the fluctuation of anisotropic magnetic interactions of the nitroxide electron spin [43–47] which can be induced by orientational motion of the nitroxide molecule as a whole. This contribution in all cases with a good accuracy was found to be approximated as exponential decay (see inset to Fig. 1), $E(2\tau) \propto \exp(-2\tau W_{\text{anis}})$, with W_{anis} as the decay rate.

The obtained W_{anis} temperature dependences are shown in Fig. 1 for the cases of solvation by pure water and by water–glycerol mixture, and for two spin-label positions, $n = 5$ and $n = 16$. One can see in Fig. 1 an abrupt increase of W_{anis} for temperatures higher than 200 K, for the all samples studied. Also one can see that solvation by pure water results in the same W_{anis} values for both label positions

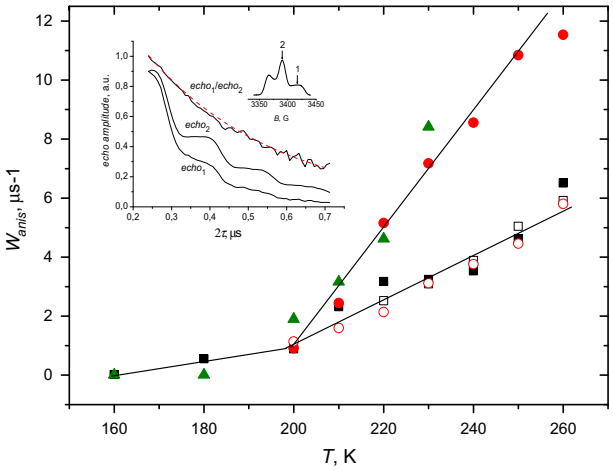

Fig. 1 *Inset*: the example of two time traces obtained at the field positions *1* and *2* (artificially adjusted to the same value at the beginning), and their ratio with its exponential approximation (*solid* and *dashed lines*, respectively). The exponential decay rates W_{anis} are given at different temperatures for DPPC bilayers prepared with spin-labeled lipids 5-PCSL (*circles*), 16-PCSL (*squares*), and with spin probe 3,4-dicarboxy-PROXYL (*triangles*). *Open symbols*—bilayer are solvated by pure water, *filled symbols*—by water–glycerol mixture (1:1 v/v). The *straight lines* are drawn to visualize the start of the W_{anis} increase

while in presence of glycerol for $n = 5$ the W_{anis} increases much faster with temperature, as compared with hydration by pure water.

Data in Fig. 1 also present the W_{anis} values obtained for spin probe 3,4-dicarboxy-proxyl, when bilayer was solvated by water–glycerol mixture. This spin probe is expected, due to its high polarity, to appear only in the solvation shell (which was directly confirmed using ESEEM spectroscopy [48]). So its motions reflect the motion of the bulk solvent surrounding. One can see the closeness of data for 3,4-dicarboxy-proxyl and for 5-PCSL.

Figure 2 shows the examples of EPR spectra (see inset) for the *n*-PCSL in DPPC bilayers. One can see that EPR spectra are transforming slightly as temperature increases. In particular, the separation between the two outmost peaks, which corresponds to twice the principle component of the hyperfine tensor, A_{zz}, is decreased with temperature. These data are collected in Fig. 2 for the both cases of solvation by pure water and water–glycerol mixture, and for both spin-label positions, $n = 5$ and $n = 16$. One can see that, first, for $n = 5$ the $2A_{zz}$ value is higher than that for $n = 16$. This result can be readily explained by a higher polarity of surrounding in the former case [49]. Second, above 230–240 K an abrupt drop of the $2A_{zz}$ temperature dependence occurs.

4 Discussion

The data presented in Fig. 1 may be interpreted within the model of stochastic nanosecond molecular librations [43, 44, 50]. Consider a nitroxide spin label experiencing fast stochastic librations around the *X* molecular axis with small

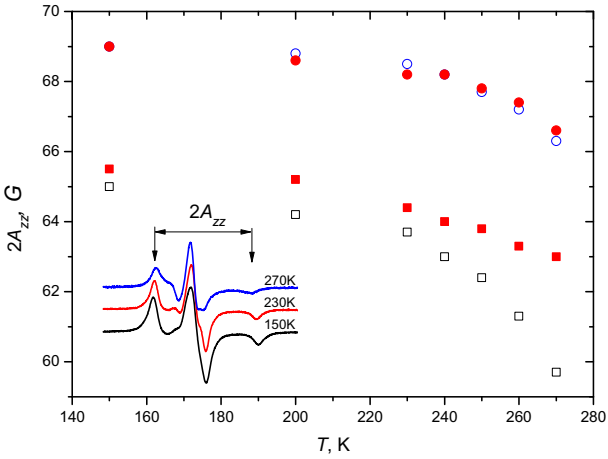

Fig. 2 Representative CW EPR spectra for DPPC bilayers (*inset*, 16-PCSL sample hydrated in pure water) and $2A_{zz}$ values obtained for spin-labeled lipids 5-PCSL (*circles*) and 16-PCSL (*squares*). *Open symbols*—solvation by pure water, *filled symbols*—solvation by water–glycerol mixture (1:1 v/v)

reorientation angle $\alpha(t)$, $\langle\alpha^2(t)\rangle \ll 1$, where angular brackets mean time averaging. The echo signal in this model decays exponentially as $E(2\tau) \propto \exp(-2\tau W_{\text{anis}})$ [44, 50], where

$$W_{\text{anis}} = \langle\alpha^2\rangle R_X^2(\theta,\varphi)\tau_c, \tag{1}$$

and

$$R_X(\theta,\varphi) = \gamma\left[B(g_{YY} - g_{ZZ}) + \frac{m(A_{YY}^2 - A_{ZZ}^2)}{(A_{XX}^2\sin^2\theta\cos^2\varphi + A_{YY}^2\sin^2\theta\sin^2\varphi + A_{ZZ}^2\cos^2\theta)^{1/2}}\right]\cos\theta\sin\theta\sin\varphi,$$

where γ is the gyromagnetic ratio; τ_c is the correlation time for motion; θ and ϕ are the angles determining the orientation of the magnetic field in the molecular framework of the nitroxide spin label; B is the magnetic field strength; g_{YY}, g_{ZZ}, A_{YY}, A_{ZZ} are the principal values of the g-tensor and the tensor of hyperfine interaction. For a small-amplitude motion, angles θ and ϕ in Eq. 1 correspond to their averaged values. For motion around the two other molecular axes, Y and Z, a circular permutation in Eq. 1 must be made of the subscripts X, Y, and Z, simultaneously with the polar coordinates $\sin\theta\cos\varphi$, $\sin\theta\sin\varphi$, and $\cos\theta$.

Fast motion means that $\langle\alpha(t)^2\rangle R_X^2(\theta,\varphi)\tau_c^2 < 1$ (that corresponds to the Redfield's limit in the theory of spin relaxation). Under the used experimental setup (the time traces at the field positions 1 and 2, see inset to Fig. 1, are divided by each other) it was shown previously [50] that the $|R_X(\theta,\varphi)|$ and $|R_Y(\theta,\varphi)|$ values in Eq. 1 may be replaced by a constant approximately equal to 2.8×10^8 s^{-1}. So fast motion means that τ_c lies at the nanosecond time range. This estimation of τ_c was directly

confirmed in three-pulse-stimulated ESE experiments on spin labels in biological membranes [46, 50]. Then we may write down an approximate simple equality:

$$W_{\text{anis}} \approx \left(10^{17}\text{s}^{-2}\right)\langle\alpha(t)^2\rangle\tau_c. \quad (2)$$

The obtained data on the product $\langle\alpha^2\rangle\tau_c$ may be compared [45] with the MSD, $\langle r^2\rangle$, obtained in neutron scattering and Mössbauer absorption experiments [15–30]. From one hand, the $\langle\alpha^2\rangle$ and τ_c cannot be obtained separately, and this is a disadvantage of the approach. On the other hand, as purely harmonic motion does not produce spin relaxation because of its dynamical nature, the onset of dynamical transition in ESE decays must be seen more clearly than in neutron scattering.

Note that lipid membranes are surrounded by two different types of water—free bulk water and water bound to the phospholipid headgroups near the surface of the bilayer, as it is known from solid-state NMR studies [51–54]. The temperature at which water bound to lipid bilayers freezes is much lower than that for free water [53]. NMR relaxation data show that water near the phospholipid headgroups remain unfrozen at temperatures as low as 200 K [54]. The molecular motion found here also shows the existence of low-temperature molecular motions near the membrane surface, with an accordance with these NMR data.

At the 5th label position, the W_{anis} value is found to be nearly the same as that for polar nitroxide spin probe assumed to be partitioned into the solvation shell—see Fig. 1. We may conclude that motion of small molecules in the bulk water–glycerol solution and motion of molecular groups in lipids near the membrane surface possess close dynamical properties in the temperature range studied. This result is in agreement with the general conclusions obtained in neutron scattering experiments and MD simulations for proteins and DNAs hydrated in presence of glycerol [20, 24, 31, 32] which established a close connection between the dynamics of side chains of biomolecules and the solvent structural relaxation.

At the 16th label position, the W_{anis} value is found to be unaffected by presence of glycerol in the solvating shell. This result can be easily understood because, according to the ESEEM data on glycerol penetration into the DPPC bilayer [48] which were obtained under the same experimental conditions, the glycerol concentration in the bilayer interior is rather small.

CW EPR spectra also are sensitive to molecular librations and dynamical transition [40, 55], because the measured splitting between the two outmost peaks (see inset to Fig. 2) corresponds not to the true $2A_{ZZ}$ value but to an effective $2\langle A_{ZZ}\rangle$ value, where $\langle A_{ZZ}\rangle$ decreases due to motional averaging [43, 44] as:

$$\langle A_{ZZ}\rangle = A_{ZZ} - \langle\alpha(t)^2\rangle(A_{ZZ} - A_{YY}) \quad (3)$$

(for motion around the X molecular axis).

However, several circumstances make the CW EPR approach less favorable for detecting dynamical transition. First, CW spectra can be easily saturated at low temperatures which results in their distortion and so introducing artifacts in the $\langle A_{ZZ}\rangle$ measurement. Second, $\langle A_{ZZ}\rangle$ values are noticeably influenced by harmonic motions [56] which persist below and above the dynamical transition temperature T_d. Third, the polarity of environment also can strongly influence $\langle A_{ZZ}\rangle$ [49], except

of molecular motion. And finally, the precision of detecting dynamical transition in CW EPR is much less than that in the ESE approach.

Indeed, in CW EPR the accuracy of $\langle A_{ZZ} \rangle$ measurements is determined by inhomogeneous EPR line broadening in glassy media which results in the uncertainty to be around 0.1–0.2 G, which in turn allows from Eq. 3 to estimate the smallest $\langle \alpha^2 \rangle$ to be measured as $\sim 5 \times 10^{-3}$ rad^2. The latter is to be compared with the sensitivity of ESE experiments which could be estimated in the following way. The experimental uncertainty of obtaining W_{anis} is $\sim 10^6$ s^{-1} (cf. Fig. 1). Then the lowest $\langle \alpha^2 \rangle$ value which can be measured is $\sim 10^{-11}/\tau_c$, as it follows from Eq. 2, and in the most favorable case of $\tau_c \sim 10^{-7}$ s (only motions with $\tau_c < 10^{-6}$ s are detected in the used ESE approach otherwise the decay is too slow and/or field independent), we arrive to the estimation $\langle \alpha^2 \rangle \sim 10^{-4}$ rad^2 which is almost two orders of magnitude smaller than in CW EPR. Generally speaking, the much better ESE sensitivity follows from the fundamental advantage of spin echo in detecting weak magnetic interactions by eliminating the inhomogeneous broadening of EPR spectral lines.

Data presented in Fig. 2 show that CW EPR spectra indeed are temperature dependent, and the spectral splitting between two outmost peaks decreases with temperature (it is denoted in Fig. 2 simply as $2A_{ZZ}$). However, the noticeable $2A_{ZZ}$ decrease starts at temperatures 230–240 K, where the W_{anis} in ESE experiments already attains rather high values (cf. Fig. 1). We relate this difference between results of two techniques with the mentioned above their different sensitivity to stochastic molecular librations and also with possible influence of increasing polarity with temperature on the A_{ZZ} measurements. (Note in that respect that in cholesterol-containing DPPC bilayers the $2A_{ZZ}$ value for 5-PCSL was found not to decrease but to increase with temperature [57]). So we may conclude that CW EPR provides information on the dynamical transition that is less pronounced and more extended in temperature, as compared with the ESE approach.

5 Conclusions

Study of molecular motions in biological systems in deeply frozen state is helpful for elucidation of the molecular mechanisms of action of cryoprotective agents, such as glycerol. ESE allows investigating fast stochastic or diffusive orientational vibrations (molecular stochastic librations) of spin labels. These measurements produce quantitative data on the molecular motions: according to Eq. 2, the motional parameter—the product of mean-squared angular amplitude and the correlation time, $\langle \alpha^2 \rangle \tau_c$, can be determined. This information resembles that obtained in neutron scattering experiments, where the MSD, $\langle r^2 \rangle$, is obtained.

The motional parameter $\langle \alpha^2 \rangle \tau_c$ here was found to be small below 200 K and to increase sharply above this temperature, for both cases of solvating by pure water and by water–glycerol mixture, and for both 5th and 16th label positions. The analogous phenomenon was observed in neutron scattering experiments on the biological membranes [27–30], where $\langle r^2 \rangle$ was found to increase sharply above ~ 200 K.

The important advantage of spin-label ESE is the possibility of obtaining data on motions at the selected sites of biomolecules, which is attained using selective labeling. Also, ESE approach, as compared with neutron scattering, possesses a higher sensitivity to the onset of dynamical transition because it is not sensitive to harmonic motion which in MSD data manifest itself as background linear temperature dependence. And finally, experiments on spin-echo EPR of spin labels are more easily accessible for experimentalists than those on neutron scattering. From the other hand, the $\langle \alpha^2 \rangle$ and τ_c values cannot be obtained separately, and this is a disadvantage.

In presence of glycerol, the motional parameter $\langle \alpha^2 \rangle \tau_c$ was found to become larger for the 5th label position, as compared with hydration by pure water, and not to change for the 16th one (above 200 K). In the former case it was found to be nearly the same as that for a polar spin probe assumed to be partitioned into the solvating shell. These results indicate that at low temperatures motion of solvating shell governs the motions of the bilayer surface and does not influence the motions in the membrane interior.

Acknowledgments This work was supported by the Russian Foundation for Basic Research (project no. 12-03-00192-a.

References

1. P. Westh, Biophys. J. **84**, 341 (2003)
2. A. Nowacka, S. Douezan, L. Wadsö, D. Topgaard, E. Sparr, Soft Matter **8**, 1482 (2012)
3. M. Akhoondi, H. Oldenhof, H. Sieme, W.F. Wolkers, Mol. Membr. Biol. **29**, 197 (2012)
4. Kyrychenko, T.S. Dyubko, Biophys. Chem. **136**, 23 (2008)
5. J.J. Towey, L. Dougan, J. Phys. Chem. B **116**, 1633 (2012)
6. P.H. Yancey, M.E. Clark, S.C. Hand, R.D. Bowlus, G.N. Somero, Science **217**, 1214 (1982)
7. P.W. Hochachka, G.N. Somero, *Biochemical Adaptation* (Princeton University Press, Princeton, 1984)
8. K.B. Storey, J.M. Storey, Comp. Biochem. Physiol. **83**, 613 (1986)
9. T.J. Anchordoguy, A.S. Rudolph, J.F. Carpenter, J.H. Crowe, Cryobiology **24**, 324 (1987)
10. A.K. Fry, A.Z. Higgins, Cell. Mol. Bioeng. **5**, 287 (2012)
11. J.G. Duman, D.W. Wu, L. Xu, D. Tursman, T.M. Olsen, Quart. Rev. Biol. **66**, 387 (1991)
12. V.G. Sakai, F. Engelmann, Cryoletters **28**, 151 (2007)
13. J.P. Acker, J.A.W. Elliott, L.E. McGann, Biophys. J. **81**, 1389 (2001)
14. P.R. Davis-Searles, A.J. Saunders, D.A. Erie, D.J. Winzor, G.J. Pielak, Annu. Rev. Biophys. Biomol. Struct. **30**, 271–306 (2001)
15. F. Parak, E. Frolov, A. Kononenko, R. Mössbauer, V. Goldanskii, A. Rubin, FEBS Lett. **117**, 368 (1980)
16. H. Keller, P. Debrunner, Phys. Rev. Lett. **45**, 68 (1980)
17. E.R. Bauminger, S.G. Cohen, I. Nowik, S. Ofer, I. Yariv, Proc. Natl. Acad. Sci. USA **80**, 736 (1983)
18. W. Doster, S. Cusack, W. Petry, Nature (London) **337**, 754 (1989)
19. W. Doster, Biochim. Biophys. Acta **1804**, 3 (2010)
20. E. Cornicchi, G. Onori, A. Paciaroni, Phys. Rev. Lett. **95**, 1581041–1581044 (2005)
21. K. Wood, A. Frolich, A. Paciaroni, M. Moulin, M. Hartlein, G. Zaccai, D.J. Tobias, M. Weik, J. Am. Chem. Soc. **130**, 4586 (2008)
22. S. Khodadadi, S. Pawlus, J.H. Roh, V.G. Sakai, E. Mamontov, A.P. Sokolov, J. Chem. Phys. **128**, 195106 (2008)
23. K.L. Ngai, S. Capaccioli, A. Paciaroni, J. Chem. Phys. **138**, 235102 (2013)
24. E. Cornicchi, S. Capponi, M. Marconi, G. Onori, A. Paciaroni, Eur. Biophys. J. **37**, 583–590 (2008)

25. J.H. Roh, R.M. Briber, A. Damjanovic, D. Thirumalai, S.A. Woodson, A.P. Sokolov, Biophys. J. **96**, 2755 (2009)
26. N.V. Surovtsev, V.K. Malinovsky, E.V. Boldyreva, J. Chem. Phys. **134**, 045102 (2011)
27. R.E. Lechner, J. Fitter, N.A. Dencher, T. Hauss, J. Mol. Biol. **277**, 593 (1998)
28. J. Fitter, R.E. Lechner, N.A. Dencher, J. Phys. Chem. **103**, 8036 (1999)
29. K. Wood, M. Plazanet, F. Gabel, B. Kessler, D. Oesterhelt, G. Zaccai, M. Weik, Eur. Biophys. J. **37**, 619 (2008)
30. F. Natali, A. Relini, A. Gliozzi, R. Rolandi, P. Cavatorta, A. Deriu, A. Fasano, P. Riccio, Chem. Phys. **292**, 455–464 (2003)
31. T.E. Dirama, G.A. Carri, A.P. Sokolov, J. Chem. Phys. **122**, 244910–244911 (2005)
32. M. Tsai, D.A. Neumann, L.N. Bell, Biophys. J. **79**, 2728–2732 (2000)
33. N.V. Surovtsev, E.S. Salnikov, V.K. Malinovsky, L.L. Sveshnikova, S.A. Dzuba, J. Phys. Chem. B **112**, 12361 (2008)
34. N.V. Surovtsev, S.A. Dzuba, J. Chem. Phys. **140**, 235103 (2014)
35. N.V. Surovtsev, N.V. Ivanisenko, K.Yu. Kirillov, S.A. Dzuba, J. Phys. Chem. B **116**, 8139 (2012)
36. I.V. Borovykh, P. Gast, S.A. Dzuba, Appl. Magn. Reson. **31**, 159–166 (2007)
37. R. Guzzi, M. Babavali, R. Bartucci, L. Sportelli, M. Esmann, D. Marsh, Biochim. Biophys. Acta **1808**, 1618–1628 (2011)
38. R. Guzzi, R. Bartucci, L. Sportelli, M. Esmann, D. Marsh, Biochem. **48**, 8343–8354 (2009)
39. F. Scarpelli, R. Bartucci, L. Sportelli, R. Guzzi, Eur. Biophys. J. **40**, 273–279 (2011)
40. D. Marsh, R. Bartucci, R. Guzzi, L. Sportelli, M. Esmann, **1834**, 1591–1595 (2013)
41. G. Romeo, Appl. Phys. A **106**, 893–900 (2012)
42. F. Varga, E. Migliardo, B. Takacs, S. Vertessy, Magazù, M. T. F. Telling, J. Biol. Phys. **36**, 207–220 (2010)
43. S.A. Dzuba, Spectrochim. Acta Part A **56**, 227–234 (2000)
44. E.P. Kirilina, S.A. Dzuba, A.G. Maryasov, Yu.D. Tsvetkov, Appl. Magn. Reson. **21**, 203–221 (2001)
45. S.A. Dzuba, E.P. Kirilina, E.S. Salnikov, J. Chem. Phys. **125**, 054502 (2006)
46. N.V. Ivanisenko, S.A. Dzuba, Appl. Magn. Reson. **44**, 883–891 (2013)
47. R. Guzzi, M. Babavali, R. Bartucci, L. Sportelli, M. Esmann, D. Marsh, Biochim. Biophys. Acta **1808**, 1618–1628 (2011)
48. K.B. Konov, N.P. Isaev, S.A. Dzuba, Mol. Phys. **111**, 2882–2886 (2013)
49. D. Marsh, Appl. Magn. Reson. **37**, 435–454 (2010)
50. N.P. Isaev, V.N. Syryamina, S.A. Dzuba, J. Phys. Chem. B **114**, 9510–9515 (2010)
51. J. Wolfe, G. Bryant, K. Koster, CryoLetters **23**, 157–166 (2002)
52. K. Ueda, H. S. Tseng, Y. Kaminoh, S.M. Ma, H. Kamaya, S. H. Lin. Mol. Pharmacol. **29**, 582–588 (1986)
53. D.-K. Lee, B.S. Kwon, A. Ramamoorthy, Langmuir **24**, 13598–13604 (2008)
54. C.-H. Hsieh, W.-G. Wu, Biophys. J. **71**, 3278–3287 (1996)
55. S.V. Paschenko, Yu.V. Toropov, S.A. Dzuba, Yu.D. Tsvetkov, A.Kh. Vorobiev, J. Chem. Phys. **110**, 8150–8154 (1999)
56. L.V. Kulik, L.L. Rapatsky, A.V. Pivtsov, N.V. Surovtsev, S.V. Adichtchev, I.A. Grigor'ev, S.A. Dzuba, J. Chem. Phys. **131**, 064505 (2009)
57. D.A. Erilov, R. Bartucci, R. Guzzi, D. Marsh, S.A. Dzuba, L. Sportelli, Biophys. J. **87**, 3873–3881 (2004)